


# Process parameter influence on texture heterogeneity in asymmetric rolling of aluminium sheet alloys

Diarmuid Shore<sup>1</sup>  · Leo A.I. Kestens<sup>2</sup> · Jurij Sidor<sup>3,4</sup> · Paul Van Houtte<sup>1</sup> · Albert Van Bael<sup>1</sup>

Received: 2 September 2016 / Accepted: 14 November 2016 / Published online: 26 November 2016  
© Springer-Verlag France 2016

**Abstract** Experimental investigations of asymmetric rolling of sheet alloys demonstrate that this process may be used to alter the crystallographic texture by the introduction of shear components. Such texture components are desirable for their potential to improve the formability of aluminium alloys in deep drawing, because they do not transform to the detrimental cube component after recrystallisation. It is however not precisely known how the process parameters affect the texture evolution and the formation of texture gradients. The results of a parametric finite element study of the deformation field and the texture evolution arising during a single pass of asymmetric cold rolling are presented together with an assessment of the impact of texture gradients on the macroscopic anisotropy determined by multi-scale modelling. The modelling approach is validated with textures measured for a single pass of asymmetric rolling of an aluminium sheet alloy. The study targets an industrially feasible process window and presents the relationships found between shear texture volume fractions, texture heterogeneity, plastic anisotropy and several types of process parameters (geometric, contact and material).

**Keywords** Asymmetric rolling · Texture evolution · Aluminium · Parametric study

## Introduction

Strong incentives exist for producers of mass market vehicles to increase fuel efficiency and reduce emissions. Despite the high specific strength of aluminium alloys, the economic balance in automotive manufacture has been in favour of steels in terms of the ease and rapidity with which they can be formed, fastened and welded. Nevertheless aluminium alloys have increasingly found application in body panels and the number of all-aluminium bodied vehicles being produced is increasing (Table 1) [1]. One obstacle to replacing steel with aluminium alloys is the relatively low formability, evident for example in forming limit diagrams (FLD) and formability parameters such as limiting dome height or limiting drawing ratio (LDR). Engler et al. partially attribute this to unfavourable plastic anisotropy arising from the typical crystallographic texture of rolled aluminium alloys [2]. The formability of an aluminium alloy sheet can be indicated by parameters such as the direction-averaged normal anisotropy  $\bar{r}$  and the power law strain hardening exponent  $n$ . Stress ratio parameters can be similarly employed, e.g. the ratio  $P$  of stress in plane strain tension to the equibiaxial stress [3] or the ratio of stress in plane strain tension to the pure shear stress [4]. Broadly speaking, increasing the value of  $\bar{r}$  increases the proportion of strain occurring in the sheet plane rather than in the thickness, implying that the thickness is reduced less during stretching. Analysis shows that the LDR is directly proportional to  $\bar{r}$  [5]. The flow rule of plasticity implies that  $\bar{r}$  is a function of the shape of the yield surface, which in turn depends on the texture, and can be derived from it using a statistical crystal plasticity (CP) model [6]. While Burger et al. report that other aspects of the microstructure such as grain morphology influence

✉ Diarmuid Shore  
diarmuid.shore@mtm.kuleuven.be

<sup>1</sup> Department of Material Engineering, KU Leuven, Kasteelpark Arenberg 44, Box 2450, 3001 Leuven, Belgium

<sup>2</sup> Department of Materials Science and Engineering, Ghent University, Technologiepark 903, B-9052 Ghent, Belgium

<sup>3</sup> Department of Mechanical Engineering, University of West Hungary, Károlyi Gáspár tér 4, Szombathely 9700, Hungary

<sup>4</sup> Department of Mechanical Engineering, Eötvös Loránd University, Károlyi Gáspár tér 4, Szombathely 9700, Hungary

**Table 1** Examples of passenger vehicles with aluminium alloy intensive body work

Manufacturer	Models	Production
Pierce Arrow	Various	1915–1929 (approx.)
BMW	328 roadster	1936–1940 (approx.)
Panhard	Dyna X, Dyna Z	1948–1959
Landrover	Defender	1948–2015
Honda	NSX	1990–2005
Audi	A8	1994–present
Audi	A2	1999–2005
Honda	Insight Hybrid	1999–present
Ford	F150	2015–present

the plastic behaviour [7], simulation results presented by Xie et al. suggest that in the current context the effects of grain shape are of second order importance [8]. It follows that statistical CP models provide an appropriate basis for the calculation of formability parameters such as  $\bar{r}$ . The Taylor-Bishop-Hill (TBH) or full constraints (FC) model [9] is commonly used as a reference CP model, though more advanced statistical models such as the ALAMEL have been shown to provide greater accuracy for aluminium alloys [10, 11]. In any case common to all statistical CP models is the valid prediction that rolled sheet steels featuring textures containing the  $\alpha$  fibre ( $\langle 110 \rangle$  || rolling direction) and  $\gamma$  fibre ( $\langle 111 \rangle$  || rolling direction) have higher  $\bar{r}$  values than rolled aluminium alloys, containing the  $\beta$  fibre, (i.e. orientations linking the copper  $\{112\} \langle 111 \rangle$ , S3  $\{123\} \langle 63\bar{4} \rangle$  and brass  $\{110\} \langle \bar{1}12 \rangle$  components) and cube  $\{100\} \langle 001 \rangle$  components.

The cube orientation is frequently the dominant texture component in recrystallised sheet aluminium alloys. CP calculations show that textures of fcc materials with a strong cube component have low values of  $\bar{r}$  relative to those with  $\beta$  fibre textures [12]. The growth of cube grains during annealing is favoured by virtue of the  $40^\circ \langle 111 \rangle$  relationship between cube and  $\beta$  fibre orientations [13]. Intermediate annealing during cold rolling may be used to mitigate cube formation during final annealing, and the magnesium content of automotive alloys promotes fragmentation of the cube bands from which cube grains nucleate [14]. On the other hand the cold deformation applied in commercially produced automotive alloys may be insufficient to suppress formation of cube during annealing by these means, though in alloys containing large constituent particles (e.g. the 6XXX series) the condition of dispersoids may be controlled so as to augment particle stimulated nucleation (PSN) [2], which promotes formation of P  $\{011\} \langle 122 \rangle$  and ND rotated cube  $\{001\} \langle 310 \rangle$  at the expense of cube [13].

Considering the above, production of novel deformation textures with higher  $\bar{r}$  values than conventional rolling textures have recently drawn the attention of researchers as a new means to improve formability. Asymmetric rolling

(ASR) is a variant of conventional rolling where the boundary conditions on the upper or lower surface are intentionally unequal, creating a zone of unidirectional shear deformation which propagates through the sheet thickness. Kim et al. report that during ASR the cube and  $\beta$  fibre components are replaced with shear components H  $\{001\} \langle 110 \rangle$ , E  $\{111\} \langle \bar{1}10 \rangle$  and F  $\{111\} \langle 112 \rangle$ , and that these are retained after annealing [15]. Engler et al. observe  $\gamma$  fibre components to persist during annealing [16]. Sakai et al. report strong shear components and elimination of cube [17], while Kang et al., Cheon et al. and Kestens et al. also report reduction of cube after ASR and annealing [18–20]. Kim et al. report the cube component decreases during ASR and further decreases during annealing, leading to high  $\bar{r}$  values [21]. In summary the above evidence supports the idea that ASR improves the formability of aluminium alloys by beneficial modification of the texture.

Sidor et al. present CP modelling results showing that shear deformation, of aluminium sheet alloys during rolling rotates the  $\beta$  fibre and cube components towards the H, E and F components, in general agreement with the experimental results. However they also experimentally observe formation of gradients in the texture [11]. Wronski et al. also observe the formation of texture gradients in ASR experiments, which do not disappear during annealing [22]. Furthermore Wronski et al. remark that a complete explanation of texture gradient formation has yet to be proposed [23].

This article presents a correlation of process parameters of a single pass of ASR with texture and texture gradient evolution, and investigates the impact of such gradients on the formability. First the experiments validating the computational approach are presented, followed by a description of the modelling approach used for a parametric study of ASR. The results are presented and discussed in the context of an industrially feasible configuration of the ASR process for aluminium alloys.

## Experiment

A conventionally produced automotive AA6016 aluminium sheet (fully annealed) is rolled in a single cold asymmetric rolling pass in a two-high laboratory mill, using rolls driven at equal angular speeds. The upper and lower rolls were 310 mm and 460 mm in diameter respectively, giving a roll surface velocity ratio of 1.5. The sheet is reduced from 1.22 mm to 1 mm thickness, corresponding to an 18% pass reduction with a ratio of the smaller roll radius to initial sheet thickness of 127. No lubrication or specific surface treatment is applied. After rolling the sheet is annealed at  $550^\circ\text{C}$  for 30 s, with recrystallisation confirmed by electron back scattered diffraction (EBSD).

The texture is measured for the three conditions (as received, deformed, annealed) on an RD-ND plane through the full thickness of the sheet using EBSD. Orientation distribution functions (ODFs) are calculated using the MTM-FHM software by superimposing Gaussian distributions with a spread of 5°, centred on the set of discrete orientations measured by EBSD. The ODF is constructed using the series expansion method introduced by Bunge [24] with  $L_{max} = 22$ , and is plotted in the space of Euler angles ( $\phi_1, \Phi, \phi_2$ ) following the convention adopted by Bunge. Monoclinic sample symmetry, appropriate for plane strain compression with shear, where TD is an axis of two-fold rotational symmetry, is assumed in the ODF calculations. For such symmetry the ODF is conveniently plotted in  $\phi_2$  sections with  $-90^\circ \leq \phi_1 \leq 90^\circ$ . Figure 1 gives the locations of the ideal orientations in such plot, including positions on the  $\{111\}$  pole figure: the location of the  $\gamma$  fibre is indicated with the dashed line in the  $\phi_2 = 45^\circ$  section. S, copper and brass are typical deformation components for conventionally rolled aluminium alloys, cube and P are typical for recrystallisation after conventional rolling, and H and F are typical for asymmetrical rolling.

The sharp texture of the as received sheet is represented in the ODF plotted in Fig. 2. The texture index is 2.2 and the ODF maximum 13.1. It is dominated by  $\{001\}\langle 100 \rangle$  (cube) oriented grains, which is typical for a recrystallised conventionally rolled aluminium alloy. There are also  $\{011\}\langle 100 \rangle$  (Goss) and weak  $\{011\}\langle 112 \rangle$  (P) components present. As touched on in the introduction the P component is understood to be associated with the occurrence of particle stimulated nucleation (PSN) during recrystallisation in AA6XXX alloys, though this is not investigated further here.

The texture of the deformed material, shown in Fig. 3, is in general weaker and notably the cube component has vanished, while distinct  $H\{001\}\langle 110 \rangle$  and  $F(111) [\bar{2}11]$  components are present. The texture index is 1.2 and the ODF maximum is 3.6. As mentioned in the introduction, rotated cube and components in the  $\gamma$  fibre such as F are expected in fcc materials undergoing significant shear during rolling.

The texture of the recrystallised material, shown in Fig. 4, is similar to the deformation texture both in terms of the main components and sharpness. The texture index is 1.2 and the ODF maximum 3.3. The texture is similar to the deformation texture (see Fig. 3), with retention of the  $\{001\}\langle 110 \rangle$  (H) component and weakening of  $(111) [\bar{2}11]$  (F). Orientations near the  $\gamma$  fibre are still present after recrystallisation. No cube component is observed.

### Modelling

As motivated in the introduction, a parametric study of the process window for ASR is conducted to correlate the process parameters of a single rolling pass with texture evolution and texture gradient evolution, and to investigate the impact of deformation texture gradients on the formability. The independent process parameters examined in the study were the material hardening coefficient  $K$ , Coulomb friction coefficient  $\mu$ , relative pass reduction ratio  $\alpha$ , ratio of lower to upper roll radii  $r_{ul}$ , ratio of upper roll radius to sheet thickness  $r_{rr}$ . The complete set of parameter values used is given in Table 2. The values of  $K$ , the coefficient of the Swift hardening law, were chosen to represent annealed AA5000 and AA6000 series alloys [25, 26] and the hardening exponent  $n$  was taken as 0.275, falling in the middle of the range typical for aluminium

**Fig. 1** Legend for the ODF and  $\{111\}$  pole figure showing ideal components

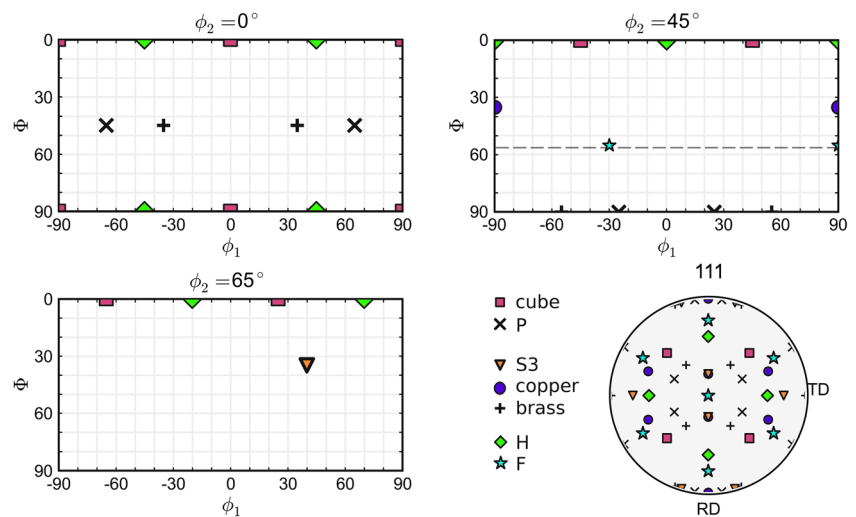
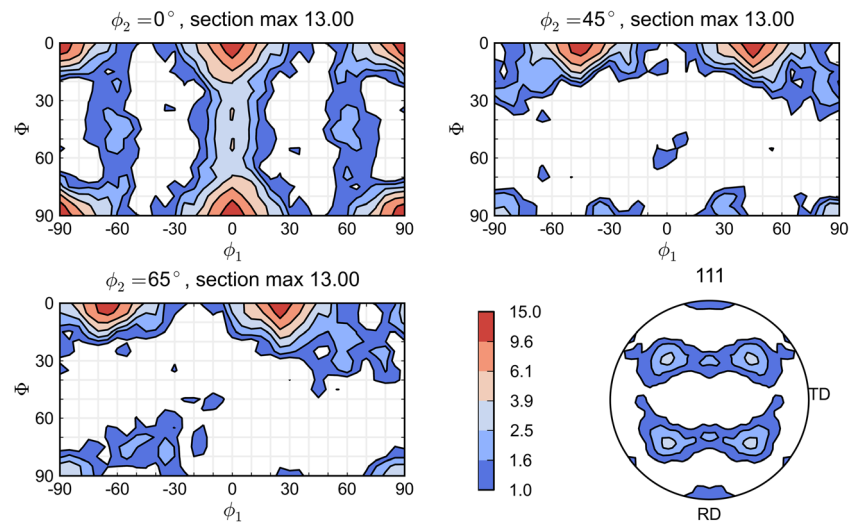


**Fig. 2**  $\varphi_2$  sections of the ODF and recalculated  $\{111\}$  pole figure representing the texture of the sheet used as starting material for the asymmetric rolling experiment



alloys. The values of  $\mu$  were chosen to be representative of rolling in industrial settings, which is conducted with lubrication in boundary or mixed regimes for reasons of roll wear minimisation, product surface finish and process stability. According to the experimental measurements of friction in rolling of aluminium by Jeswiet et al. conducted without lubrication [27], and those of Tabary et al. and Lenard and Zhang with lubrication [28, 29] and the experimental results discussed by Lenard et al. [30], the range  $0.02 \leq \mu \leq 0.2$  is assumed to be appropriate for this scenario. The values of  $r_{ul}$  were chosen to range from symmetric to significantly asymmetric rolling. The values of  $\alpha$  represent reductions from somewhat above a “skin pass” to close to the limit for a single pass in cold rolling of aluminium. The values of  $r_{rt}$  were chosen to represent a range of rolling from that of relatively thick sheet (or use of relatively small rolls)  $r_{rt} = 10$  to relatively thin sheet (or use of large rolls)  $r_{rt} = 30$ : in this way

heterogeneity developing in the earlier stages of cold rolling is explored, noting that many laboratory investigations have used small rolls (e.g. 100 mm radius) but with thin sheet (e.g. 1 mm) which may be more representative rather of the final stages of cold rolling. A full factorial design is used giving  $2(K) \times 4(\mu) \times 4(\alpha) \times 4(r_{ul}) \times 3(r_{rt}) = 384$  configurations to simulate.

Considering the large number of finite element and crystal plasticity calculations required to explore the process window, the following computationally efficient material models were employed: (i) the ALAMEL crystal plasticity model [10], (ii) the FACET method introduced by Van Houtte et al., which uses a convex plastic potential calibrated with a CP model as an anisotropic yield criterion for finite element analysis of metal forming [31] and (iii) the Hierarchical Multi Scale (HMS) framework introduced by Gawad et al. which connects and coordinates models operating at various length scales in a

**Fig. 3**  $\varphi_2$  sections of the ODF and recalculated  $\{111\}$  pole figure representing the experimental texture of the sheet after deformation

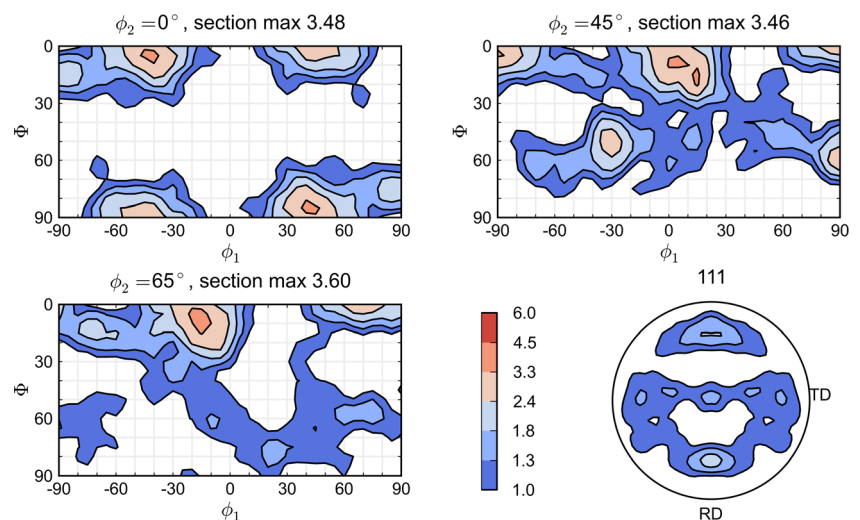
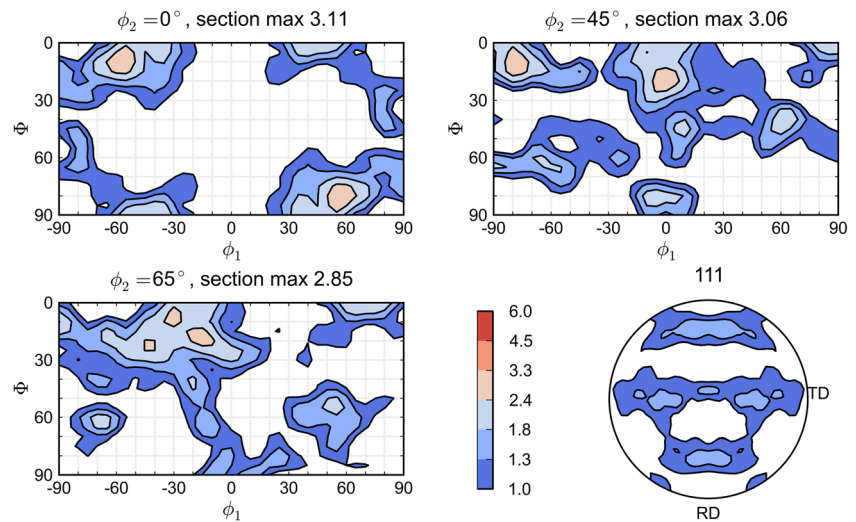


**Fig. 4**  $\varphi_2$  sections of the ODF and recalculated {111} pole figure representing the experimental texture of the sheet after recrystallisation annealing



manner which retains accuracy while minimising computational cost [32].

The Taylor Bishop Hill (TBH) model is a statistical model of crystal plasticity which assumes each grain in a polycrystal deforms homogeneously with the macroscopically applied strain, as discussed by Van Houtte et al. [33]. ALAMEL modifies the TBH model to account for the heterogeneity of plastic deformation by considering the cooperative deformation of grains along common boundaries [31]. The model considers a planar boundary, and the adjacent sub regions of the two grains sharing this boundary, as a system which collectively conforms to the macroscopic deformation, but permits the components parallel to the boundary plane of the respective velocity gradients, within both grain regions, to be varied in tandem to achieve shear stress equilibrium along that boundary. The model characterises the boundary and grain regions by their orientations and allows for these to evolve during a simulation. A large number of such grain and grain boundary orientations are considered so that the effects of grain interactions and microstructure evolution are accounted for in a statistical manner. Kanjarla et al. present crystal plasticity finite element method (CPFEM) simulations which demonstrate that adjacent regions in grains tend to shear along the grain boundaries, and that the deformation mode local to the boundary extends into the grain interiors, which supports the validity of the assumptions of the ALAMEL model [34].

The FACET method, as used here with the assumption of a rate insensitive material, takes the form of a homogenous polynomial of degree  $n$  representing a yield surface in deviatoric stress space, per Eq. 1. The  $\lambda_k$  and  $D_k^p$  terms are parameters: the  $D_k^p$  represent plastic strain rate modes (directions in strain rate space) for which the corresponding  $\lambda_k$  are weighting factors. The  $D_k^p$  are chosen to cover strain rate space with a particular angular resolution, and the  $\lambda_k$  are found by a non-negative least squares algorithm which fits the

FACET expression to the results of virtual mechanical tests (CP simulations) as discussed by Gawad et al. [32].

$$\phi(S) = \left( \sum_{k=1}^K \lambda_k (S : D_k^p)^n \right)^{\frac{1}{n}} = 1, \quad \lambda_k \geq 0 \quad (1)$$

The inequality condition in Eq. 1 guarantees convexity of the expression. In the present case 2482 strain modes  $D_k^p$ , equally spaced in the five dimensional deviatoric strain rate space are employed in the calibration. The degree  $n$  of the polynomial must be an even natural number greater than 2, and controls the smoothness of the surface: in the present case  $n = 8$  is used based on the recommendations of the original authors. This type of model has the advantage that apart from the initial calibration procedure it reproduces the full anisotropic response of the underlying crystal plasticity model without the associated computational expense, making it suitable for implementation in explicit finite element analysis where typically millions of evaluations of the model are required.

A schematic of the parametric model of ASR is presented in Fig. 5. It may be described in two parts, namely the isotropic model of the single pass ASR process itself and the evolution of texture (steps a and b), and the calculation of resulting properties due to the texture and texture gradients (steps c to g). Analysis step (a) is conducted with the commercial FEM software Abaqus/Explicit version 6.13, which implements a displacement driven updated Lagrangian approach. The explicit solver is employed because of its robust contact modelling. Four node bilinear plane strain elements with reduced integration (first order ‘‘CPE4R’’ element type) were used for the deformable sheet material. Between ten and twenty element layers were used in the sheet thickness direction, depending on the value of  $r_{ub}$ , giving meshes with 1000 to 2500 elements. An example mesh is partially shown in

**Table 2** Independent parameter values used in the parametric study of asymmetric rolling

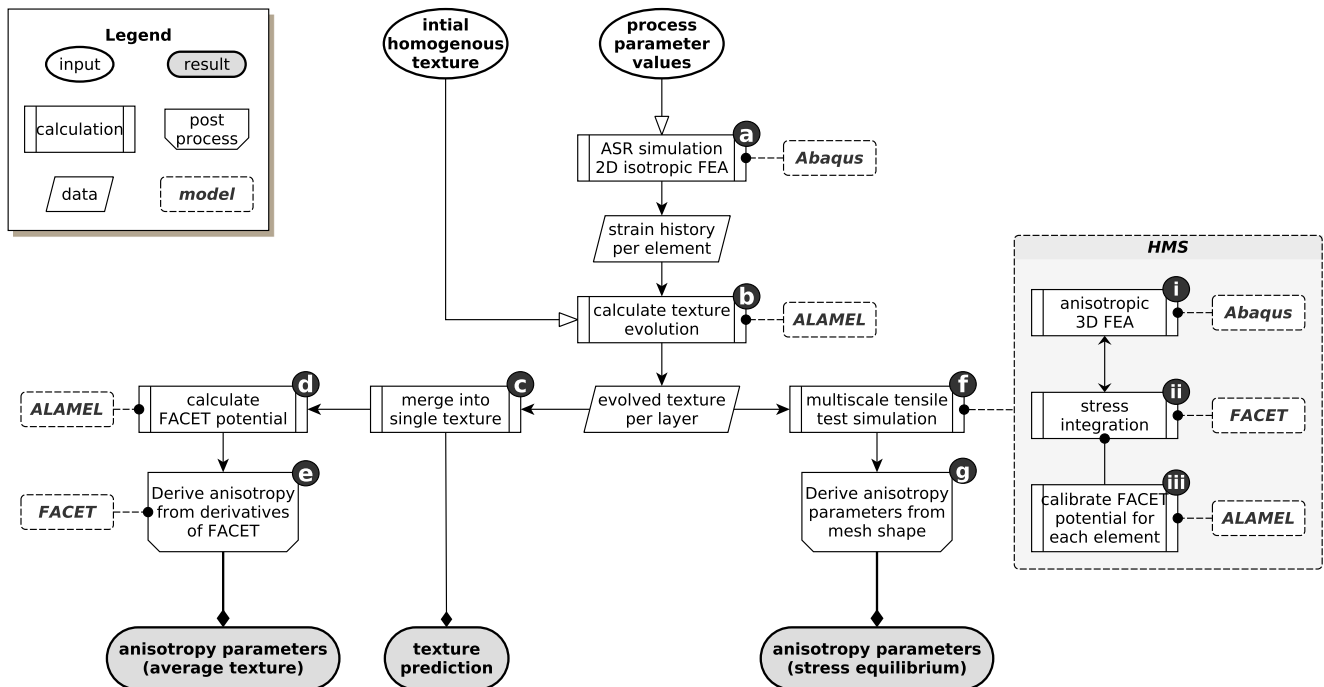
Parameter	Symbol	Values	Unit
Strain hardening coefficient	$K$	$2.78 \times 10^8, 6.92 \times 10^8$	Pa
Coulomb friction coefficient	$\mu$	0.02, 0.05, 0.1, 0.2	Dimensionless
Relative pass reduction	$\alpha$	0.1, 0.2, 0.3, 0.4	Dimensionless
Roll radius ratio (upper/lower)	$r_{ul}$	1.0, 1.25, 1.5, 1.75	Dimensionless
Upper roll radius to sheet thickness ratio	$r_{rt}$	10, 20, 30	Dimensionless

Fig. 6 for reduction of 40% with a roll ratio of 1.5 and  $r_{ul}=30$ . The rolls were modelled with a single layer of rigid quadrilateral elements (“R2D2” element). Contact between the rigid rolls and sheet is handled by the Abaqus/explicit general contact algorithm using a linear contact pressure overclosure relationship with the large sliding penalty based method for tangential stresses.

The Abaqus scripting interface is used to build models for each of the 384 process configurations. The scripted approach allowed certain algebraic relationships between the independent and dependent parameters to be prescribed. For example the initial element aspect ratio is a function of the prescribed reduction to minimise mesh distortion, the element size is a function of the sheet thickness, the roll element size is a function of the sheet element size, the sheet initial velocity is a function of the roll velocity and simulation duration, the sheet length is a function of the thickness and the largest roll radius, etc. Considering that the explicit technique is used and the material is modelled as rate independent, the simulation

duration, which along with element size largely dictates the wall clock time per simulation, is determined by calculating the roll velocities which would lead to rolling of the whole sheet with a maximum estimated strain rate below 100 - Ginzburg et al. discusses an analysis in which this strain rate value is a guide in terms of avoiding strain rate effects in real rolling processes [35], however quasi-static conditions were also verified by confirming the kinetic energy is below 5% of the energy dissipated in plastic work in each simulation. Mass scaling is not employed.

The entry angle  $\phi$  of the sheet to the roll gap is controlled in a specific way: the sheet is made to run through two horizontal rigid frictionless guides which have only the vertical degree of freedom unconstrained, so that the sheet is restricted to be strictly horizontal everywhere before entry into the roll gap, but is otherwise free to determine its equilibrium position in the vertical direction with respect to the rolls. The local reduction (the proportion of the reduction applied by a given roll) calculated using Eqs. 2, 3 and 4 suitably prescribes the initial



**Fig. 5** Schematic of the parametric model of texture development in ASR

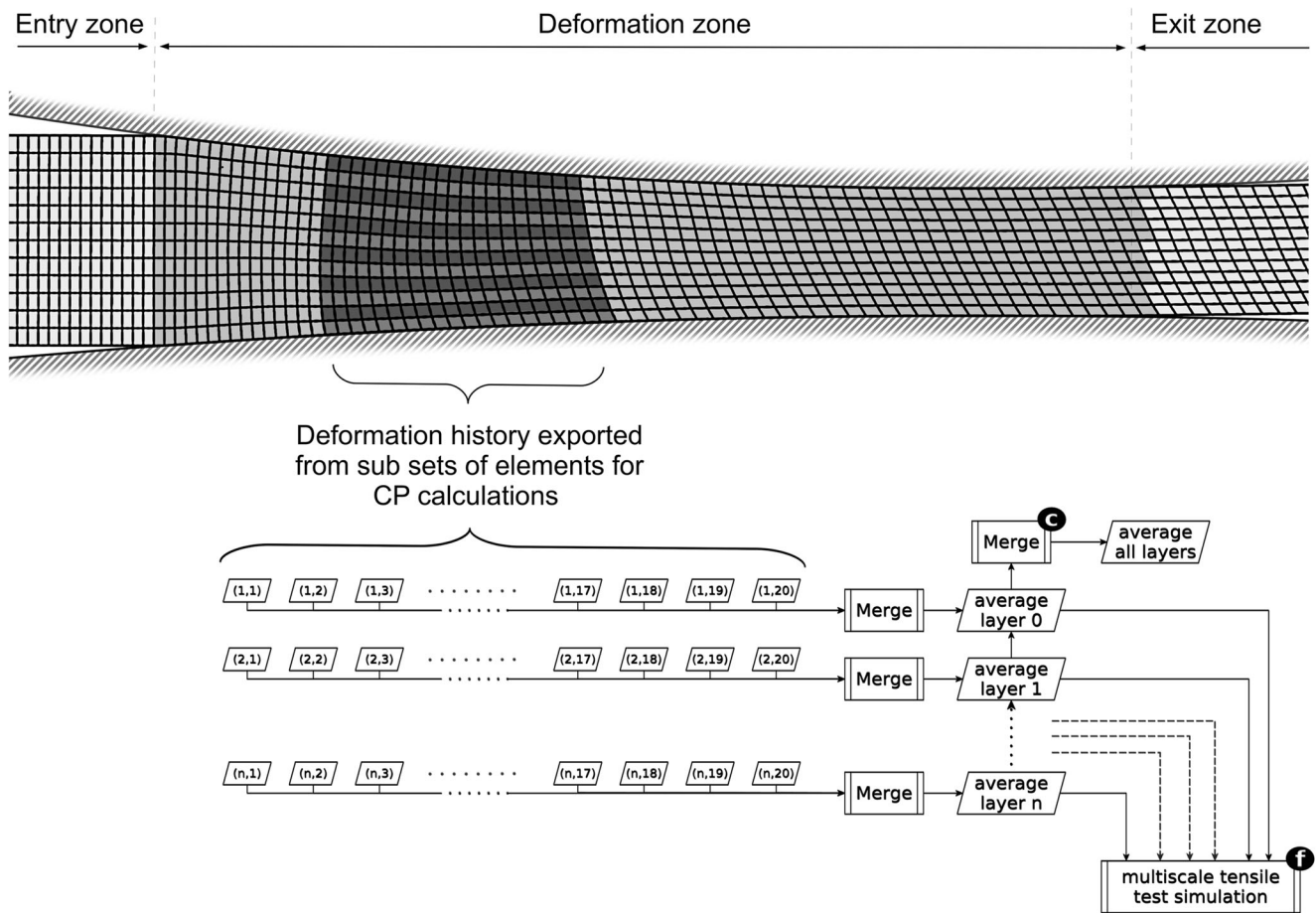


**Fig. 6** An example of part of a mesh used in the 2D FE analysis of a single pass of ASR with 40% reduction and roll ratio of 1.5 together with a schematic indicating the method of merging predicted ODFs where the modules labelled (c) and (f) correspond with those of Fig. 5

vertical position of the sheet to within a fraction of the element edge length of the equilibrium position, and it is found that equilibrium is achieved by the moment that the leading edge of the sheet began to leave the roll gap.

$$\Delta h = h_i - h_f = \Delta h_1 + \Delta h_2 \tag{2}$$

$$\Delta h_1 = \frac{\Delta h(2R_2 - \Delta h)}{2(R_1 + R_2 - \Delta h)} \tag{3}$$

$$\Delta h_2 = \frac{\Delta h(2R_1 - \Delta h)}{2(R_1 + R_2 - \Delta h)} \tag{4}$$

The nodal positions of elements in a 20 x n element “zone of interest” in the sheet mesh, covering the full thickness of the sheet (see Fig. 6, where n refers to the number of elements in the sheet thickness direction), were exported at 100 evenly spaced time steps (each step represented about 1000 increments of the explicit solver). This zone was positioned such that the stress and strain fields within it were not influenced either by transient conditions during first contact of the sheet with the rolls, or by the free surfaces at the leading and trailing

edge of the sheet, following the general principle discussed by Montmitonnet et al. that the distance from the point of interest to the sheet end should exceed at least twice the initial sheet thickness [36]. The element shape functions were used to interpolate the nodal displacements within each element from one step to the next, from which deformation gradients for the element centroid could be derived (relevant example usage of shape functions is elaborated in Bhavikatti’s text on the finite element method [37]). With reference to Fig. 5: in step b the texture evolution is calculated with respect to the fixed reference system of the rolling process (rolling direction, transverse direction and sheet normal direction, referred to hereafter as RD, TD and ND) at each step using the ALAMEL crystal plasticity model for each of the elements in the zone of interest. The texture represented in the ODF of Fig. 2 is used as the initial texture for all calculations. As outlined in the schematic in Fig. 6, the final representative texture for each horizontal RD-TD layer of elements is calculated by merging the 20 final textures belonging to this layer.

Following this the plastic anisotropy of the material for each point in the parametric study is assessed in two ways. The first method, referred to hereafter as the “average texture”

method, calculates a single texture by merging the representative texture for each layer of elements (step c in Fig. 5), followed by calibration of a FACET potential function (step d) from which values for  $r(\theta)$  defined by Eq. 5 are derived, (step e in Fig. 5); results obtained in this manner thus represent the predicted anisotropy of a hypothetical sheet with a homogeneous texture which is the average of the graded texture through the thickness.

$$r(\theta) = \frac{\varepsilon_{\text{width}}}{\varepsilon_{\text{thickness}}} \quad (5)$$

The second method, referred to hereafter as the “multi-scale method”, uses the anisotropic hierarchical multi-scale model (HMS) to simulate the tensile test (Fig. 5 step f). In this HMS model Abaqus/Explicit is employed to model a cross section of a tensile test sample with 3D first order continuum “C3D8R” elements (Fig. 5, step f, part i); each horizontal layer of elements in the tensile sample is assigned a unique anisotropic FACET plastic potential (step f, part ii) which is calibrated using the ALAMEL CP model operating on a texture taken from the corresponding layer in the simulated rolled sheet (step f, part iii). A single layer of 3D elements, i.e. a layer one element deep in the tensile extension direction, spanning the tensile sample width and thickness directions was used. In fact the mesh is arranged so that there are three times as many elements in the thickness direction of the tensile sample as in the corresponding rolling simulation - this is done in order to allow for a gradient in strain in each layer of the tensile test simulation to accommodate contrast in material properties between adjacent layers (the linear reduced integration elements in Abaqus do not permit a gradient in strain across the element). The size in the tensile sample thickness direction matches the size of its corresponding layer in the simulated rolled material. Strain hardening is set to the same initial state as for the rolling simulations, in effect simulating a tensile test of a fully recovered material where the texture has not been altered by recrystallisation. Boundary conditions are specified such that the sheet ND is a two-fold rotational axis of symmetry for the process. Displacement of the nodes along the tensile direction is prescribed, and all other degrees of freedom are otherwise unconstrained, apart from the anchoring of a reference node. The ratio of the total logarithmic strains in the tensile sample width and thickness directions, i.e. the  $r(\theta)$  values per Eq. 5, are calculated at a logarithmic tensile strain of 0.15 for tensile test simulations at  $15^\circ$  intervals in the range  $0^\circ \leq \theta \leq 90^\circ$  with respect to the rolling direction. The strains are calculated using the displacements of the surfaces of the simulated tensile sample, in analogy to a conventional extensometer measurement: this approach was chosen in anticipation of curvature of the external surfaces arising from the variation in plastic anisotropy from one layer to the next in the tensile sample, a phenomenon which Van Bael et al. observed experimentally in tensile tests of steels with texture

gradients [38]. However it was subsequently found that the magnitude of this curvature is not significant for the purpose of anisotropy calculation for the simulations conducted in this study.

## Validation

The simulations presented in this article make use of a number of simplifications regarding the material behaviour and boundary conditions which are assumed to have negligible or second order effects on the evolution of the texture. It is thus necessary to demonstrate to what degree the texture can be predicted with this approach. The normalised error integral (EI) quantifies the difference between an experimental ODF  $f_{\text{exp}}$  and a predicted ODF  $f$ , and a value of EI = 0 indicates perfect agreement.

$$EI(f) = \frac{\oint (f - f_{\text{exp}})^2 dg}{\oint f_{\text{exp}}^2 dg} \quad (6)$$

As friction is not quantified in the experiment, a value for the friction coefficient  $\mu$  is determined by calculating the value of EI as a function of  $\mu$  for simulations matching the geometry of the experiment with  $\alpha = .2$ ,  $r_{ul} = 1.5$ ,  $K = 692\text{MPa}$ ,  $r_{rt} = 127$ . The result is plotted in Fig. 7, and is compared with results obtained with the Taylor (TBH) model.

Calculations using the ALAMEL model consistently produce better agreement with the experimental texture than the TBH model. The best texture predictions with ALAMEL are obtained with  $\mu \geq 0.3$ .  $\mu = 0.3$  is a physically plausible value for the experiment considering that it is conducted without lubrication. The average through thickness texture for the model of ASR with  $\alpha = .2$ ,  $r_{ul} = 1.5$ ,  $K = 692\text{MPa}$ ,  $\mu =$

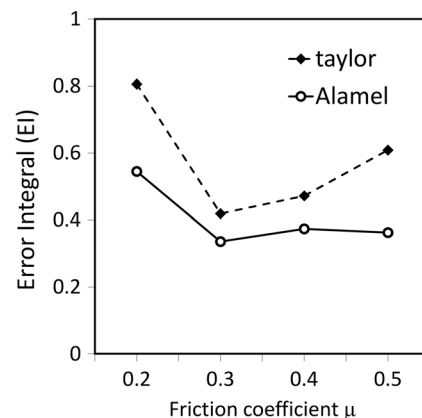


**Fig. 7** The effect of the friction coefficient on the quality of the texture prediction quantified in terms of the normalised error integral of Eq. 6 with other process parameters chosen to match the experimental conditions



0.3,  $r_{rt} = 127$  is presented in Fig. 8. The texture index is 1.4 and ODF maximum 4.1. There is good qualitative agreement between the FE based simulation and the experiment: the appearance of the F and H components, and disappearance of the Goss and P are correctly predicted. The quantitative comparison ( $EI = 0.31$ ) indicates a valid result, however the cube component while weakened has not vanished as observed in the experiment.

### Results

The first objective of the study is to examine the effect of the ASR process parameters on the plastic anisotropy: Fig. 9 presents box plots of  $\bar{q}$  values (related to  $\bar{r}$  by Eq. 7) which summarise the results of the parametric study with relative pass reductions  $0.2 \leq \alpha \leq 0.4$ , categorised by  $\alpha$ .  $\bar{q}$  values are used in preference to  $\bar{r}$  because they are constrained to take values  $0 \leq \bar{q} \leq 1$ . The results of the two calculation methods, described earlier as the “average texture” and “multi-scale” methods, are represented as the shaded and clear boxes respectively.

$$\bar{q} = \frac{1}{1 + \bar{r}} \quad (7)$$

The boxplots are of the conventional type where the upper, lower and middle horizontal lines of the boxes represent the upper and lower quartiles, and the median respectively of the of the relevant data, while the whiskers represent minimum and maximum values, excluding outliers; outliers are defined as those values greater than 1.5 times the upper or lower quartiles. While both sets of data show the same trend with respect to reduction, the multi-scale method results exhibit lower spread and show higher magnitudes compared to the average texture method. The calculated  $\bar{q}$  value for the experimental deformed texture (0.466) is marked with a star symbol in

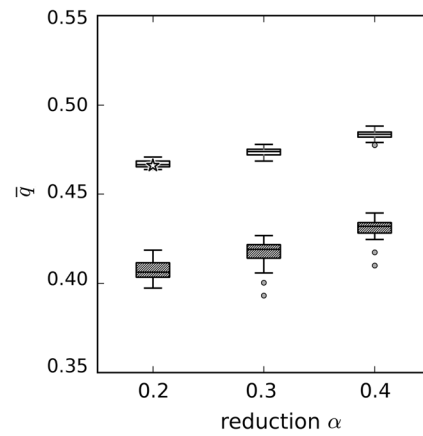
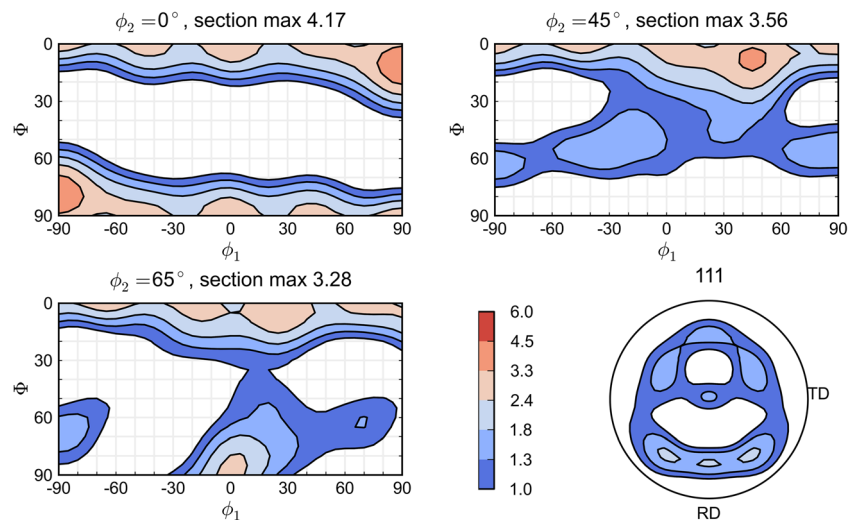


**Fig. 9** Box plot of  $\bar{q}$  values as a function of reduction calculated with the “average texture” (shaded) and “multi-scale” methods (clear) where the predicted  $\bar{q}$  value of 0.46 for the experimental deformed texture is marked with a star symbol

Fig. 9 and falls within the range of values predicted by the multi-scale method. The anisotropy, as assessed by  $\bar{q}$  value, appears sensitive mainly to the reduction, and for the whole parametric study is confined within a small range- nevertheless, it is essential to bear in mind that this result concerns the anisotropy of the material in the deformed condition, and that it is only after recrystallisation during annealing that the texture changes unique to ASR are expected to have a dramatic effect on the anisotropy.

The second objective then is to examine the correlation of process parameters with texture volume fractions, in particular those of the  $\beta$  and  $\gamma$  fibres. The volume fraction of grains with the orientation of an ideal texture component is estimated as the total integral over the Euler space of the product of the ODF and a model function, divided by the value by the maximum of the model function (in this case the model function is an ODF constructed by applying a Gaussian spread of 11 degrees on an ideal orientation of interest). The volume

**Fig. 8**  $\phi_2$  sections of the predicted ODF and  $\{111\}$  pole figure for the model configuration corresponding to that of the experiment (i.e. the ODF calculated as the average of all the ODFs for the individual layers in the rolled sheet)



fraction of the  $\beta$  fibre is calculated here simply as the sum of the volume fractions of copper, brass and S3, while that of the  $\gamma$  fibre as the sum of E and F components.

A general correlation with roll radius ratio is illustrated in Fig. 10 where the volume fractions of  $\gamma$  and  $\beta$  fibre components are expressed as a function of roll ratio  $r_{ul}$ , ranging from conventional rolling ( $r_{ul} = 1$ ) to highly asymmetric rolling ( $r_{ul} = 1.75$ ) for a sub set of the data with pass reduction  $\alpha \geq 0.2$  and friction  $\mu = 0.2$ . The volume fractions of the  $\beta$  and  $\gamma$  fibres in the initial texture are 0.09 and 0.01. As may be expected the  $\beta$  fibre volume fraction increases significantly over the starting value for symmetric rolling, while it is unchanged or decreased for asymmetric rolling. The volume fractions of  $\beta$  fibre and  $\gamma$  fibres in the experimental deformed texture (10% and 5.5% respectively, marked with the star and diamond symbols in Fig. 10) agree with the predicted volume fractions. While the optimal increase in  $\gamma$  fibre and decrease in  $\beta$  fibre volume fractions is achieved with the largest process asymmetry  $r_{ul} = 1.75$ , the spread in results is greater than at  $r_{ul} = 1.5$ , suggesting that texture development is more sensitive to change in the process parameter values at high asymmetry.

Decreasing the friction coefficient, even to  $\mu = 0.1$  (see Fig. 11) appears to eliminate any clear correlation as shear strain is reduced below the level sufficient to form  $\gamma$  fibre components, due to lower contact shear stresses.

Considering a single level of reduction, e.g. for  $\alpha = 0.4$  and  $\mu = 0.2$  as shown in Fig. 12, reveals a correlation between the ratio of roll radius to sheet thickness  $r_{rt}$  and the volume fractions: low values of  $r_{rt}$  (i.e. rolling thick sheet or using small rolls) are significantly less effective at reducing the  $\beta$  fibre and increasing the  $\gamma$  fibre than high values of  $r_{rt}$ .

This effect of the ratio of roll radius to sheet thickness is also reflected in the texture heterogeneity. The heterogeneity of texture can be quantified by Eq. 8 as  $\Delta f$ , which is the maximum of the values of the squared difference of an ODF for a given layer  $f_i$  with the average ODF for all layers  $f_{avg}$  - the larger the value of  $\Delta f$ , the larger the texture gradient

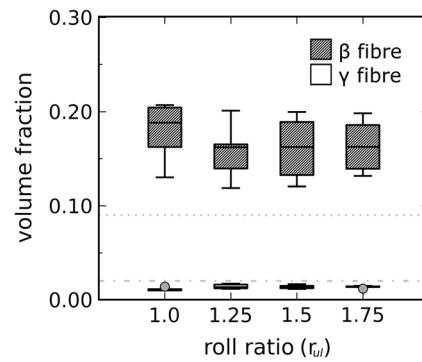


Fig. 11 Volume fractions of  $\gamma$  and  $\beta$  fibre components for average textures of the parametric study for reductions  $\alpha \geq 0.2$  and friction  $\mu = 0.1$

present in a given simulated sheet.

$$\Delta f = \max \left( \oint (f_i - f_{avg})^2 dg \right) \tag{8}$$

In Fig. 13 it is clear that the heterogeneity of texture decreases with increasing ratio of roll radius to sheet thickness  $r_{rt}$ . Together with Fig. 12 this can be interpreted to imply that at low values of  $r_{rt}$  the contact length is low and shear strain is localised at the surface of the sheet, while at higher values the contact length is greater and the shear strain penetrates toward the central layer of the sheet and thus has a stronger impact on the texture.

### Discussion

It was established during validation that a friction coefficient of value  $\mu \geq 0.3$  is required for the average ODF of the relevant simulations to agree best with that derived from the EBSD measurements. Such a value of  $\mu$  is reasonable for the non lubricated conditions of the experiment, and indeed researchers such as Lee and Lee have experimented with non-lubricated asymmetric cold rolling and found comparable

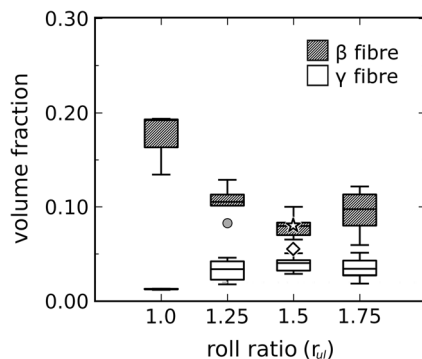


Fig. 10 Boxplot of volume fractions of  $\gamma$  and  $\beta$  fibre components for average textures of the parametric study for all simulations with reductions  $\alpha \geq 0.2$  and friction  $\mu = 0.2$  where the volume fractions of the  $\gamma$  and  $\beta$  fibres in the experimental deformed texture are marked with a diamond and star symbol respectively

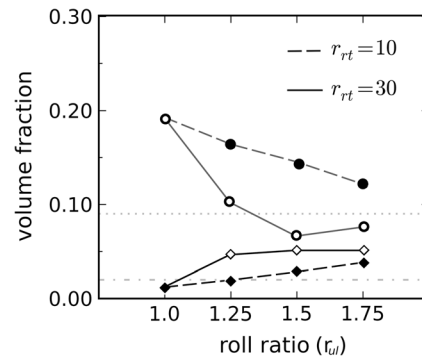
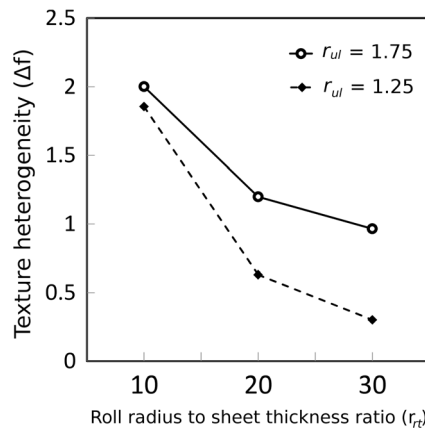


Fig. 12 The effect of the ratio of roll radius to sheet thickness  $r_{rt}$  on the volume fraction of  $\beta$  (grey lines with circle markers) and  $\gamma$  fibre (black lines with diamond markers) for a reduction of  $\alpha = 0.4$  with friction  $\mu = 0.2$ , as a function of roll ratio  $r_{ul}$



**Fig. 13** Texture heterogeneity  $\Delta f$  of Eq. 8 expressed as a function of the ratio of roll radius to sheet thickness for two levels of roll radius ratios, for a reduction of  $\alpha = 0.4$  with friction  $\mu = 0.2$

values  $0.3 \leq \mu \leq 0.5$  to be most appropriate for their simulations [39]. However use of such high friction would likely be problematic in a large scale production scenario, which motivates the parametric study of the process window of  $0.02 \leq \mu \leq 0.2$  for lubricated rolling.

The discrepancy between the texture predicted by FE based approach and the experiment, specifically the retained cube component, could in part be due to the fact that the plastic behaviour of an aluminium sheet with a rolling texture is well known to be more accurately described by an anisotropic yield surface than the isotropic von Mises law used in this study: depending on the texture anisotropic yield surfaces may feature lower yield stresses under shear compared with the prediction of the isotropic von Mises model, which would result in greater shear strain for a given frictional shear stress. Further texture measurements resolving the gradient in texture for the ASR experiment are required for a more comprehensive assessment.

Such considerations aside, on the basis that the plastic anisotropy is predicted with satisfactory accuracy, the results of the parametric study suggest that in general for the process window considered only modest gains in  $\bar{q}$  (likewise  $\bar{r}$ ) value over conventional rolling are expected in a single pass by virtue of the effects of deformation texture evolution alone, and that the magnitude of this change is chiefly a function of the amount of reduction. However the fact that asymmetric rolling and conventional rolling are predicted here to produce such similar  $\bar{q}$  values risks disguising the fact that they also appear to produce significantly distinct textures for many process configurations when sufficient friction is present (i.e.  $\mu = 0.2$  in the present case, see Fig. 10). As discussed in the introduction reducing  $\beta$  fibre components and promoting shear texture components such as orientations in the  $\gamma$  fibre is beneficial as doing so is expected to reduce the detrimental cube orientation formed by recrystallisation during annealing.

It is also important to note that the impact of texture gradients characteristic of ASR on the mechanical properties is predicted to be very low when assessed by the multi-scale method, in the sense that though the texture heterogeneity may vary significantly with process parameters for a given pass reduction (such as plotted in Fig. 13), the mechanical properties show practically no influence of these parameters. This implies either that the various deformation textures have similar mechanical properties, or that the contrast in properties is smoothed out when stress equilibrium between layers is permitted. However this behaviour may change after annealing if certain layers assume different recrystallisation textures which amplify the mechanical property contrast. In any case the  $\bar{q}$  values derived from a single (through thickness averaged) texture are consistently lower than corresponding values derived from the multi-scale model which accounts for a texture gradient, and appear to be more sensitive to variation of the process parameters for a given reduction.

Finally, it is clear that while the current results identify beneficial configurations of ASR for formability improvement in terms of modification of the deformation texture, it is crucial to quantify the behaviour of materials with such textures and texture gradients during recrystallisation. In this way an appropriate model of the texture transformation occurring during recrystallisation such as presented by Sidor et al. [40] would provide insight for the most promising process configurations for industrial application.

## Conclusions

For an industrial process window with lubricated conditions the parametric study conducted here predicts the value of  $\bar{q}$  in the deformed state for a cold asymmetrically rolled aluminium alloy is largely controlled by the reduction. When the texture gradient is taken into account in a manner allowing for stress equilibrium between layers with contrasting mechanical properties, the apparent influence of the various process parameters on  $\bar{q}$  is further attenuated. Nevertheless it is predicted that with industrially feasible process conditions ASR can produce a  $\gamma$  fibre, in particular variants of the F component, and that it also significantly attenuates  $\beta$  fibre components otherwise formed during rolling. In general this beneficial effect on texture increases with increasing difference in roll radii, increasing friction and increasing reduction per pass. The rate of improvement of the  $\bar{q}$  value diminishes and the sensitivity to process parameters increases when the roll radius ratio is increased above 1.5. The  $\bar{q}$  values derived from a single (through thickness averaged) texture are consistently lower than corresponding values derived from the multi-scale model which accounts for a texture gradient, and appear to be more sensitive to variation of the process parameters for a given reduction. Increasing the ratio of roll radius to sheet thickness

is predicted to decrease texture heterogeneity and increase the penetration of shear strain through the sheet thickness. In general modelling of recrystallisation texture transformation such as presented by Sidor et al. [40] is required to quantify the expected beneficial impact of the predicted shear texture components on the plastic properties after annealing.

**Acknowledgements** The authors wish to acknowledge the support of the Belgian IAP Inter-university attraction poles program P7/21, the KU Leuven IOF Knowledge Platform project KP/12/007, and the Research Foundation Flanders (FWO) and the Flemish Government, department EWI for provision of computational resources via the VSC (Flemish Supercomputer Center). Diarmuid Shore gratefully acknowledges the Flanders Innovation & Entrepreneurship Agency (VLAIO, formerly the Flemish government agency for Innovation by Science and Technology IWT) for provision of the doctoral scholarship number 121550.

#### Compliance with ethical standards

**Conflicts of interest** The authors declare that they have no conflict of interest.

## References

- Cantor B, Grant P, Johnston C (2008) Automotive engineering: lightweight, functional and novel materials. CRC Press, Boca Raton
- Engler O, Hirsch J (2002) Texture control by thermomechanical processing of AA6xxxAl-Mg-Si sheet alloys for automotive applications - a review. *Mater Sci Eng A* 336:249–262
- Lian, J., Barlat, F., Baudelet, B. (1989) Plastic behaviour and stretchability of sheet metals. Part II: effect of yield surface shape on sheet forming limit. *Int J Plast* 5: 131–147.
- Vegter H, ten Horn CHLJ, An YG (2008) Modeling of the plastic material behavior in advanced sheet metal forming simulations. In: Proceedings of the international symposium of automotive sheet metal forming. Jamshedpur, pp. 7–18
- Leu DK (1997) Prediction of the limiting drawing ratio and the maximum drawing load in cup-drawing. *Int J Mach Tools Manuf* 37:201–213
- Van Houtte P, Van Bael A, Winters J (1995) The incorporation of texture-based yield loci into elasto-plastic finite element programs. *Textures Microstruct* 24:255–272
- Burger G, Gupta A, Jeffrey P, Lloyd D (1995) Microstructural control of aluminum sheet used in automotive applications. *Mater Charact* 35:23–39
- Xie Q, Eyckens P, Vegter H, Moerman J, Van Bael A, Van Houtte P (2013) Polycrystal plasticity models based on crystallographic and morphologic texture: evaluation of predictions of plastic anisotropy and deformation texture. *Mater Sci Eng A* 581:66–72
- Bishop JFW, Hill R (1951) A theoretical derivation of the plastic properties of a polycrystalline face-centred metal. *Philos Mag J Sci* 42:1298–1307
- Van Houtte P, Li S, Seefeldt M, Delannay L (2005) Deformation texture prediction: from the Taylor model to the advanced Lamel model. *Int J Plast* 21:589–624
- Sidor J, Miroux A, Petrov R, Kestens L (2008) Controlling the plastic anisotropy in asymmetrically rolled aluminium sheets. *Philos Mag* 88:3779–3792
- Sidor J, Miroux A, Petrov R, Kestens L (2008) Microstructural and crystallographic aspects of conventional and asymmetric rolling processes. *Acta Mater* 56:2495–2507
- Hirsch J, Al-Samman T (2013) Superior light metals by texture engineering: optimized aluminum and magnesium alloys for automotive applications. *Acta Mater* 61:818–843
- Humphreys FJ, Hatherly M (2004) Recrystallization and related annealing phenomena, 2nd edn. Elsevier, London
- Kim KH, Lee DN, Choi C (1999) The deformation textures and Lankford values of asymmetrically rolled aluminium alloy sheets. In: Proceedings of the Twelfth International Conference on textures of materials, p 755–760
- Engler O, Kim HC, Huh MY (2001) Formation of {111} fibre texture in recrystallised aluminium sheet. *Mater Sci Technol* 17: 75–86
- Sakai T, Hamada S, Saito Y (2001) Improvement of the r-value in 5052 aluminum alloy sheets having through-thickness shear texture by 2-pass single-roll drive unidirectional shear rolling. *Scr Mater* 44:2569–2573
- Kang SB, Min BK, Kim HW, Wilkinson DS, Kang J (2005) Effect of asymmetric rolling on the texture and mechanical properties of AA6111-aluminum sheet. *Mater Trans A* 36:3141–3149
- Cheon BH, Kim HW, Lee JC (2011) Asymmetric rolling of strip-cast Al–5.5 Mg–0.3Cu alloy sheet: effects on the formability and mechanical properties. *Mater Sci Eng A* 528:5223–5227
- Kestens L, Sidor J, Petrov R, Nguyen Minh T (2012) Texture control in steel and aluminium alloys by rolling and recrystallization in non-conventional sheet manufacturing. *Mater Sci Forum* 715-716: 89–95
- Kim HK, Kim HW, Cho JH, Lee JC (2013) High-formability Al alloy sheet produced by asymmetric rolling of strip-cast sheet. *Mater Sci Eng A* 574:31–36
- Wronski S, Ghilianu B, Chauveau T, Bacroix B (2011) Analysis of textures heterogeneity in cold and warm asymmetrically rolled aluminium. *Mater Charact* 62:22–34
- Wronski S, Bacroix B (2014) Microstructure evolution and grain refinement in asymmetrically rolled aluminium. *Acta Mater* 76: 404–412
- Bunge HJ (1982) Texture analysis in material science. Butterworths, London
- Atlas of Stress Strain Curves (2002) 2nd. Edn. ASM International
- MIL-HDBK-5J (2003) Metallic materials and elements for aerospace vehicle structures US Department of Defense
- Jeswiet J (1998) A comparison of friction coefficients in cold rolling. *J Mater Process Technol* 80-81:239–244
- Tabary PE, Sutcliffe MPF, Porral F, Deneuille P (1996) Measurements of friction in cold metal rolling. *J Tribol* 118:629–636
- Lenard J, Zhang S (1997) A study of friction during the lubricated cold rolling of an aluminum alloy. *J Mater Process Technol* 72:293–301
- Lenard JG (2007) Primer on flat rolling. Elsevier, London
- Van Houtte P, Yerra SK, Van Bael A (2009) The facet method: a hierarchical multilevel modelling scheme for anisotropic convex plastic potentials. *Int J Plast* 25:332–360
- Gawad J, Van Bael A, Eyckens P, Samaey G, Van Houtte P, Roose D (2013) Hierarchical multi-scale modeling of texture induced plastic anisotropy in sheet forming. *Comput Mater Sci* 66:65–83
- Van Houtte P (1988) A comprehensive mathematical formulation of an extended Taylor–Bishop–Hill model featuring relaxed constraints, the Renouard–Wintemberger theory and a strain rate sensitivity model. *Textures Microstruct* 8:313–350
- Kanjarla AK, Van Houtte P, Delannay L (2010) Assessment of plastic heterogeneity in grain interaction models using crystal plasticity finite element method. *Int J Plast* 26:1220–1233
- Ginzburg VB (2009) Flat rolled steel processes. CRC Press, Boca Raton

36. Montmitonnet P (2006) Hot and cold strip rolling processes. *Comput Methods Appl Mech Eng* 195:6604–6625
37. Bhavikatti SS (2010) *Finite element analysis*. New Age International, New Delhi
38. Van Bael A, Hoferlin E, Kestens L, Van Houtte P (1998) Side-bulging during tensile tests of IF-steels with cross-thickness texture gradients. *Mater Sci Forum* 273-275:417–424
39. Lee JK, Lee DN (2008) Texture control and grain refinement of AA1050 Al alloy sheets by asymmetric rolling. *Int J Mech Sci* 50: 869–887
40. Sidor JJ, Kestens LAI, Decroos K, Petrov RH, Kestens LAI (2015) Evolution of recrystallization textures in particle containing Al alloys after various rolling reductions: experimental study and modeling. *Int J Plast* 66:119–137